



HAL
open science

Study of the α -Mechanical Relaxation in Molecular Glass-Forming Liquids

A. Faivre, L. David, J. Perez

► **To cite this version:**

A. Faivre, L. David, J. Perez. Study of the α -Mechanical Relaxation in Molecular Glass-Forming Liquids. Journal de Physique II, 1997, 7 (11), pp.1635-1650. 10.1051/jp2:1997207 . jpa-00248540

HAL Id: jpa-00248540

<https://hal.science/jpa-00248540>

Submitted on 4 Feb 2008

HAL is a multi-disciplinary open access archive for the deposit and dissemination of scientific research documents, whether they are published or not. The documents may come from teaching and research institutions in France or abroad, or from public or private research centers.

L'archive ouverte pluridisciplinaire **HAL**, est destinée au dépôt et à la diffusion de documents scientifiques de niveau recherche, publiés ou non, émanant des établissements d'enseignement et de recherche français ou étrangers, des laboratoires publics ou privés.

Study of the α -Mechanical Relaxation in Molecular Glass-Forming Liquids

A. Faivre (*), L. David and J. Perez

Groupe d'Études de Métallurgie Physique et de Physique des Matériaux (**),
Bâtiment 502, Institut National des Sciences Appliquées de Lyon, 20 avenue A. Einstein,
69621 Villeurbanne Cedex, France

(Received 7 March 1997, received in final form 20 July 1997, accepted 18 July 1997)

PACS.62.40+i – Anelasticity, internal friction, stress relaxation, and mechanical resonances

PACS.65.70+y – Thermal expansion and density changes; thermomechanical effects

PACS.83.20.Di – Microscopic (molecular) theories

Abstract. — A procedure yielding to the determination of the low-frequency dynamical behavior of glass-forming systems with low glass transition temperature is presented in this paper. The liquids are injected in an inorganic porous medium and the mechanical response of the heterogeneous composite samples is studied. It is shown that the dynamic behavior of the liquid is poorly affected by the presence of the substrate. This enables to build the long-time relaxation diagram for maltitol, sorbitol and LiCl, 6H₂O. The mechanical measurements are interpreted in the framework of a model based on the assumptions of localized disorder (defects) and hierarchically constrained dynamics in the glass transition region.

Nomenclature

T_g : glass transition temperature

$G^*(\omega, T)$: complex shear modulus

$G'(\omega, T)$: storage shear modulus

$G''(\omega, T)$: loss shear modulus

$\tan \phi$: loss tangent

G_r : relaxed modulus

G_u : unrelaxed modulus

$J^*(\omega, \tau)$: dynamic shear compliance

J_u : unrelaxed shear compliance

J_r : relaxed shear compliance

f_p : fraction of pore in the substrate

f_{p0} : fraction of pores remaining empty in the composite sample

τ_i : characteristic relaxation time τ_i

(*) Author for correspondence (e-mail: afaivre@dpm.univ-lyon1.fr)

(**) UMR CNRS 5510

g_i	: weight of each relaxational event having the characteristic time τ_i
χ	: parameter giving the effectiveness of the correlation effects
χ'	: second exponent in the biparabolic model
Q	: parameter of the biparabolic model closed to unity
C_d	: concentration of quasi-point defects
τ_β	: time of the simplest elementary motion involved in α -molecular mobility
τ_{mol}	: most probable relaxation time involved in the α -molecular mobility
$B_{\alpha\text{vp}}$: parameter giving the width of the distribution of τ_i in the long time range
$B_{\alpha\text{an}}$: parameter giving the width of the distribution of τ_i in the short time range
E_β	: apparent activation energy of the β -relaxation process
E_{app}	: apparent activation energy of the α -relaxation process in the glassy state
a	: parameter giving the temperature dependence of $\chi(T)$
m, m'	: fragility parameters
$G_{\text{Al}_2\text{O}_3}$: polycrystalline alumina shear modulus
$\lambda_1, \phi_1, \lambda_2, \phi_2$: series-parallel coupling parameters
G_p	: porous alumina substrate shear modulus
G_{eff}	: effective unrelaxed shear modulus of maltitol in porous alumina
G_{um}	: unrelaxed shear modulus of pure maltitol
G_{uc}	: unrelaxed shear modulus of the composite
$G_c^*(i\omega, T)$: complex shear modulus of the composite sample
$G_m^*(i\omega, T)$: complex shear modulus of maltitol
$G_{\text{eff}}^*(i\omega, T)$: effective complex shear modulus of maltitol in porous alumina

1. Introduction

The molecular motions below and through the liquid-glass transition temperature T_g are well-known to result in relaxation phenomena when some stimulus (dielectric, magnetic or mechanical field) is applied [1]. The main α -mechanical relaxation has been extensively studied in the case of (i) inorganic glasses, such as selenium [2] or oxides mixtures [3], (ii) metallic glasses [4], and (iii) polymeric organic systems [5]. During a long time, such studies were carried out by measuring the dynamic modulus by means of various techniques and describing the results in the general frame of linear viscoelasticity [6]. Then, some progress was obtained by using the time-temperature superposition principle and master curves. Among the first attempts to relate experimental aspects of the α -mechanical relaxation to physical processes occurring at the molecular level, we proposed a theory [7] based on quasi-point defects (qpd), hierarchically correlated molecular motions (hcmm) and shear microdomains (smd) concepts. This theory was successfully applied to analyze results obtained with a wide variety of amorphous polymers [8] and silicates glass-forming systems [9]. Some efforts were made in the case of water based glass-forming systems [10], but data are still needed for molecular glasses, especially in the low temperature range, *i.e.* below and close to the glass transition.

The purpose of this paper is to give new information about the α -mechanical relaxation in two types of molecular hydrogen bonded systems: polyols (sorbitol and maltitol) and an electrolytic solution LiCl, 6H₂O. Although viscosity measurements are easy to perform as soon as the system becomes liquid, studies of α -mechanical relaxation through the glass transition are more difficult. Two different situations are encountered. When T_g is higher than room

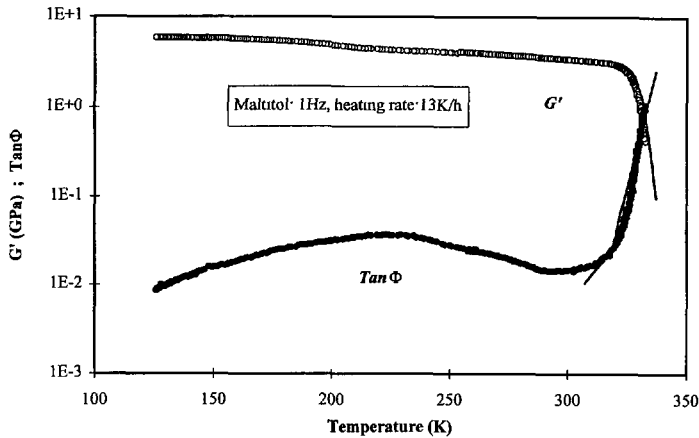


Fig. 1. — Mechanical loss tangent $\tan \phi$ and shear storage modulus G' of bulk maltitol measured as a function of temperature at 1 Hz. The full line corresponds to the modeling obtained by means of equations (3, 4 and 5) with parameters given in.

temperature, solid samples can be used for dynamic mechanical measurements, but when T_g is below room temperature, the material under study has no rigidity and must be injected in a porous solid substrate, so that measurements are performed on a composite specimen. The problem is then to extract data proper to the glass-forming liquid from the results obtained with the whole composite specimen.

2. Experimental Procedure

Low frequency dynamic mechanical spectroscopy measurements were obtained by means of a home-made inverted forced torsional oscillation pendulum described elsewhere [11]. It measures the dynamic modulus $G^*(\omega, T) = G'(\omega, T) + iG''(\omega, T)$, in helium atmosphere. The internal friction $\tan \phi$ is defined as the ratio G''/G' . Two kinds of experiments were performed. Isochronal measurements were carried out at 1 Hz as a function of temperature from 100 K to above the glass transition. Isothermal experiments were obtained at a fixed temperature in the frequency range $[1 - 10^{-4} \text{ Hz}]$.

The samples are parallelepipedal with size close to $1.5 \times 4 \times 50 \text{ mm}^3$. All samples were prepared in argon atmosphere in order to prevent hydration of the products. Bulk specimens of maltitol were molded while composite samples were obtained by injecting maltitol, sorbitol or $\text{LiCl} \cdot 6\text{H}_2\text{O}$ in a substrate cut in porous alumina [12]. The volume fraction of pores f_p in this substrate is 80%, and the average pore size is close to $3 \mu\text{m}$. It was previously verified that no relaxation process occurs in this porous substrate in the temperature range of our studies.

3. Dynamic Modulus and Molecular Mobility of Pure Maltitol

The variation of both storage G' and internal friction $\tan \phi = G''/G'$ with temperature is shown in Figure 1. The α -mechanical relaxation clearly appears above 320 K and results in an abrupt increase of $\tan \phi$ and decrease of G' . At lower temperature, between 130-300 K, a broad secondary or β -relaxation is observed. In this paper, we will focus on the α -relaxation, and Figures 2a and 2b exhibit the isothermal measurements of the dynamic modulus *versus* frequency associated with this relaxation process. The master curves obtained by shifting each of the spectra of Figures 2a and 2b along the frequency axis are displayed by Figures 3a

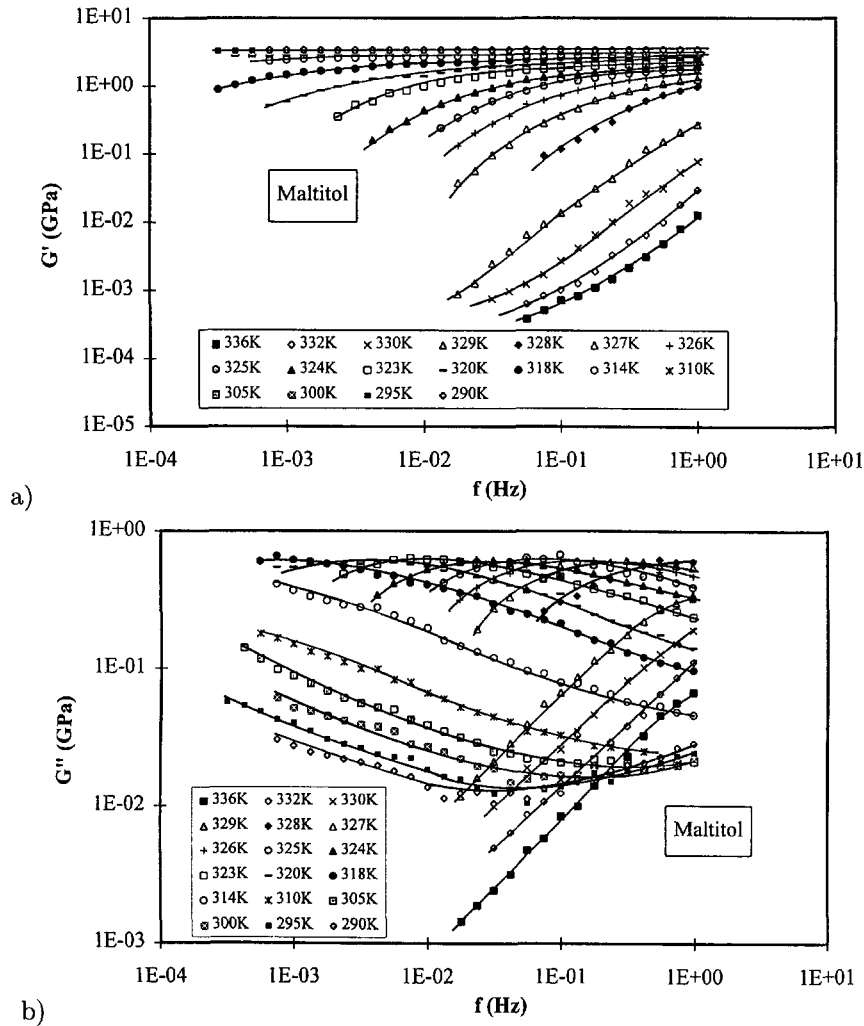


Fig. 2. — a) Frequency spectrum of the shear storage modulus G' at various temperatures for bulk maltitol. b) Frequency spectrum of the shear loss modulus G'' at various temperatures for bulk maltitol.

and 3b respectively. These data are also shown in the so-called Cole-Cole diagram (Fig. 4). We propose to analyze these results using expressions with physical sense and enlightening events occurring at nanoscale level.

First of all, it is important to note that experimental data can be treated in two different ways. One can either analyze complex susceptibilities (mechanical J^* , or dielectric ϵ^*) or complex rigidities ($G^* = 1/J^*$, or $M^* = 1/\epsilon^*$). The use of the same empirical relations for the modeling of susceptibilities or rigidities is misleading, as the values of the parameters are not directly comparable. Thus, it is necessary to be careful in the interpretation of the parameters used to fit experimental data, specially when such an interpretation is related to processes occurring at molecular level.

Several manners of describing the α -mechanical relaxation are found in literature. First, in the framework of linear viscoelasticity, the generalized Maxwell model implies the following

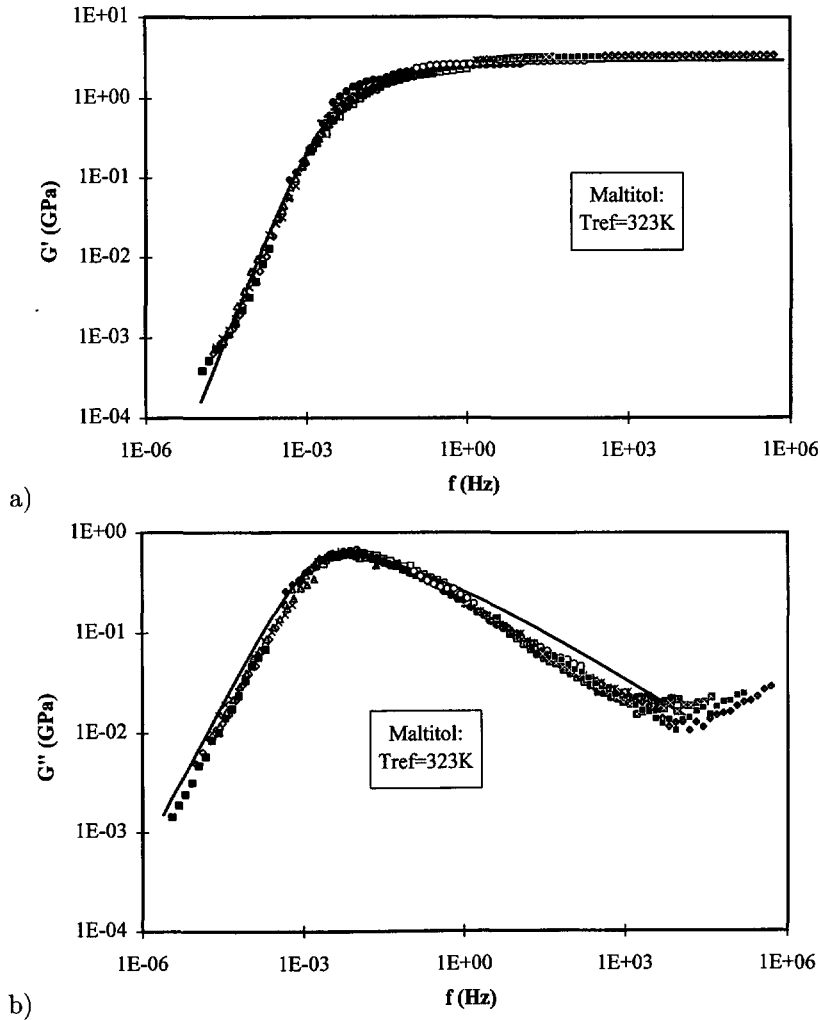


Fig. 3. — a) Master curve at 323 K built with the data displayed in Figure 2a. The full line corresponds to the modeling obtained with biparabolic model. b) Master curve at 323 K built with data of G'' measured at various temperatures and displayed in Figure 2b. The full line corresponds to the modeling obtained with biparabolic model.

relation for the complex modulus $G^*(\omega, \tau)$:

$$\frac{G^*(\omega, \tau) - G_r}{G_u - G_r} = \sum_{i=1}^n \frac{g_i j\omega\tau_i}{1 + j\omega\tau_i} \tag{1}$$

G_r and G_u are respectively the relaxed and unrelaxed moduli. g_i is the weight of the relaxational event with characteristic time τ_i , with the normalization condition $\sum_{i=1}^n g_i = 1$. The knowledge of the discrete distribution function $g(\tau_i)$ is required for using equation (1) which corresponds to a formal approach with only poor physical content.

Havriliak and Negami [13] analyzed dielectric relaxation in glass-forming liquids with the so-called H.N. relation:

$$\frac{\varepsilon^*(\omega, \tau) - \varepsilon_u}{\varepsilon_r - \varepsilon_u} = \frac{1}{(1 + (j\omega\tau)^\alpha)^\beta} \tag{2a}$$

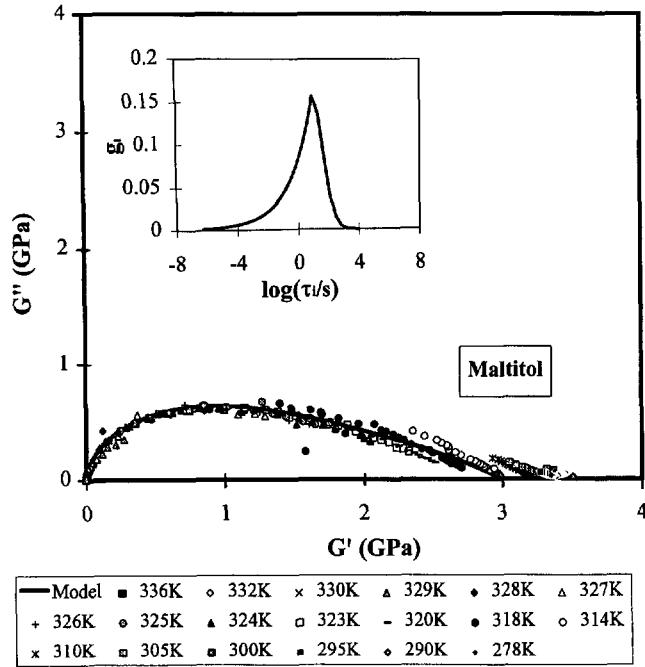


Fig. 4. — Cole-Cole representation of the data displayed in Figures 2a and b. The full line corresponds to the modeling obtained with equation (3). *Insert*: distribution of the relaxation times τ , obtained with equation (A.1) (Appendix) and the parameters given in Table I.

Equivalently, in mechanical spectroscopy:

$$\frac{J^*(\omega, \tau) - J_u}{J_r - J_u} = \frac{1}{(1 + (j\omega\tau)^\alpha)^\beta} \quad (2b)$$

$J^*(\omega, \tau)$, J_u and J_r are respectively the dynamic, unrelaxed and relaxed compliances. Equation (2) has been shown to correspond to any physical situation implying relaxational phenomena with a distribution of exponential decay. The parameter α is related to the width of the relaxation process, while β is significant of the skewness of the process. The parameters α et β must obey the conditions: $0 \leq \alpha \leq 1$, and $0 \leq \alpha^*\beta \leq 1$. It is worthwhile to note that equation (2) yields to others well-known equations: Debye ($\alpha = \beta = 1$), Cole-Cole [14] ($\beta = 1, 0 \leq \alpha \leq 1$), which is practically equivalent to the Fuoss-Kirkwood [15] or the Gaussian functions, and Cole-Davidson [16] ($\alpha = 1, 0 \leq \beta \leq 1$) functions. Alvarez *et al.* [17] have studied the relationship between the frequency-domain H.N. relation and the Kohlraush, Williams and Watts (K.W.W.) relaxation function often used in time-domain. They found that a specific K.W.W. exponent corresponds to a specific H.N. α, β pair. On the contrary, Havriliak and Negami [18] showed that the K.W.W. function can not be considered as an "universal" function, as it is not possible to find a K.W.W. exponent for every α, β couple.

Another expression, called biparabolic model, is often used to describe the dynamic modulus [19]:

$$\frac{G^*(\omega, \tau) - G_r}{G_u - G_r} = \frac{1}{1 + (i\omega\tau)^{-x} + Q(i\omega\tau)^{-x'}} \quad (3)$$

A useful comparison [20] was made between H.N. function and biparabolic expression. Although this equation (3) contains one more parameter than equation (2), it appears no

Table I. — Values of the parameters involved in the modeling of the complex dynamic modulus of bulk maltitol, by means of biparabolic model and generalized Maxwell model (Appendix).

Pure Maltitol	G_u (GPa)	G_r (GPa)	χ	χ'	Q	$B_{\alpha an}$	$B_{\alpha vp}$
Biparabolic model	3	0	0.34	1	0.3	—	—
Generalized Maxwell Model	3	0	—	—	—	0.35	0.22

significant differences in fitting the data with H.N. or biparabolic models. But the interest of biparabolic model arises from the fact that the parameters introduced in this expression can be related to physical features of the material. Equation (3) was firstly introduced as a pure formal expression, but has later been justified thanks to a theory describing the physical processes occurring in the matter when an external mechanical field is applied [7,21]. In short, the main assumptions of this theory are:

(i) the existence of quasi-point defects (qpd) in concentration C_d given by the Boltzmann statistics, corresponding to nanofluctuations of specific volume, *i.e.* enthalpy and entropy;

(ii) the hierarchically constrained nature of molecular dynamics which leads to the following expression for the characteristic time for molecular mobility in the disordered condensed matter:

$$\tau_{mol} = t_0 \left(\frac{\tau_\beta}{t_0} \right)^{1/\chi} \quad (4a)$$

$$\text{with } \tau_\beta = \tau_{0\beta} \exp \left(\frac{E_\beta}{kT} \right) \quad (4b)$$

where τ_β is the time of the simplest elementary motions involved in deformation process and identified with the sub- T_g β -relaxation motions; t_0 is a time scaling parameter, and χ is the correlation parameter ($0 < \chi < 1$) accounting for the hierarchy of the molecular mobility. Moreover, χ increases with the disorder (*i.e.* C_d) which means that χ is constant in the glassy state ($T < T_g$) implying an Arrhenius temperature dependence of τ_{mol} . On the contrary, in the supercooled liquid state, C_d and χ , increases with temperature resulting in a non-Arrhenius variation of τ_{mol} with T , which is alternatively often described with a Vogel-Fulcher-Tammann equation or William-Landel-Ferry formula;

(iii) under the application of a stress, the nucleation and growth of local shear micro domains (smd). Those smd carry the anelastic strain, involving characteristic times distributed between τ_β and τ_{mol} , and can ultimately merge irreversibly leading to viscoplastic strain, with characteristic time about τ_{mol} . Macroscopic steady deformation or flow regime appears when smd's nucleation rate and their transformation rate into viscoplastic sites become equal.

The theory summarized above yields equation (3) through relations describing the smd's nucleation, growth and coalescence. In practice, the parameters χ and χ' are easily obtained from the so-called Cole-Cole diagram exhibiting G'' versus G' , since they determine the high and low frequency limit slopes of this plot. χ varies generally between 0.2 to 0.4, and χ' is about 0.8-0.9 for amorphous polymers [8], 0.5-0.7 for highly cross-linked polymers, and 1 for non-polymeric glasses [9]. We choose to describe our results in the framework of this theory and so, equation (3) was used to fit the data of Figures 3a, 3b, and 4 with the values of parameters given in the Table I. In Figures 3b and 4, in high frequency domain, equation (3) do not lead to a perfect agreement with experimental data. The Cole-Cole diagram clearly shows non thermorheological simplicity, as the values of the unrelaxed modulus and the high frequency slope depend on the temperature of the isothermal scan. A better description of

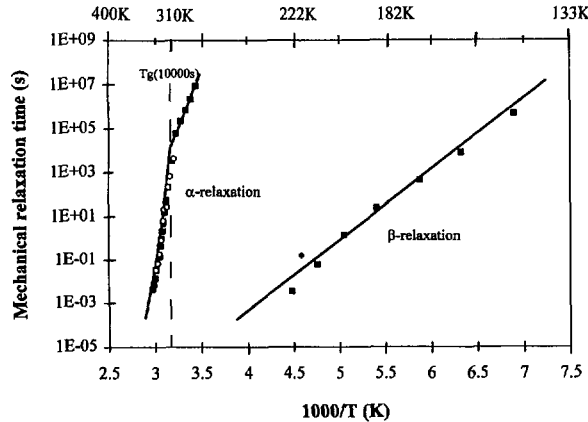


Fig. 5. — Characteristic relaxation times deduced from isothermal dynamic mechanical measurements for bulk maltitol (■) and maltitol embedded in porous alumina (○). The characteristic time deduced from isochronal measurement is also shown (◆) in Figure 1. The full lines are the result of equation (4a) and (4b), corresponding respectively to the α and β -relaxation processes.

these phenomena could be obtained by introducing the sensitivity of parameters Q and G_u to the microstructure, *i.e.*, to χ .

From isothermal measurements, it is possible to follow the variation of τ_{mol} with temperature assuming that $\omega\tau_{\text{mol}} = 1$ when G'' is maximum. For temperatures at which the maximum is not observed in the experimental frequency range, the shift factors yielding master curves are used to extrapolate the value of τ_{mol} . Figure 5 displays the variation of $\log(\tau_{\text{mol}})$ versus reciprocal temperature. Two domains can be clearly distinguished with different temperature dependence, above and below a temperature of 316 K, corresponding to a time of about 10^4 s. This temperature is referred to as $T_g = T_g(10^4 \text{ s})$, as it corresponds to the freezing of the microstructure on the time scale of experimental measurements. For $T < T_g$, in the isostructural regime, data obey an Arrhenius behavior with a slope yielding an apparent activation energy E_{app} close to 185 kJ/mol. At T_g , an abrupt change can be observed since $E_{\text{app}}(T = T_g)$ is as high as 590 kJ/mol, and for $T > T_g$, E_{app} decreases when the temperature increases.

With equation (4), it is possible to explain quantitatively the whole diagram displaying $\log(\tau_{\text{mol}})$ versus $1/T$ (Fig. 5). (i) On the one hand, from the experimental value of the activation energy of sub- T_g β -relaxation $E_b = 62$ kJ/mol and $E_{\text{app}} = 185$ kJ/mol determined in the isostructural domain, one obtains $\chi(T < T_g) = 0.33$. The value is in good agreement with that of χ calculated from the high frequency limit of the Cole-Cole diagram and given in Table I. (ii) On the other hand, it is possible to suggest [21] an explicit phenomenological temperature dependence of $\chi(T)$ through $C_d(T)$, but it is simpler to consider a Taylor expansion of $\chi(T)$ above $T_g(10^4 \text{ s})$:

$$\chi(T) = \chi(T_g) + a(T - T_g). \quad (5)$$

Data in the metastable liquid domain are consistent with a value of parameter a equal to $7.5 \times 10^{-3} \text{ K}^{-1}$. By combining equations (4 and 5) together with equations (3), it is possible to calculate the variation of the dynamic modulus with temperature and frequency through the α -relaxation. Figures 1, 3a and 3b show that such calculated curves fit correctly the respective experimental isotherms and isochrones, in a manner self-consistent with the general theoretical frame recalled above.

For a comparison with an approach involving times distribution, the equation (1) is used as explained in Appendix. Such an equation fits the data as well as equation (3), with the values

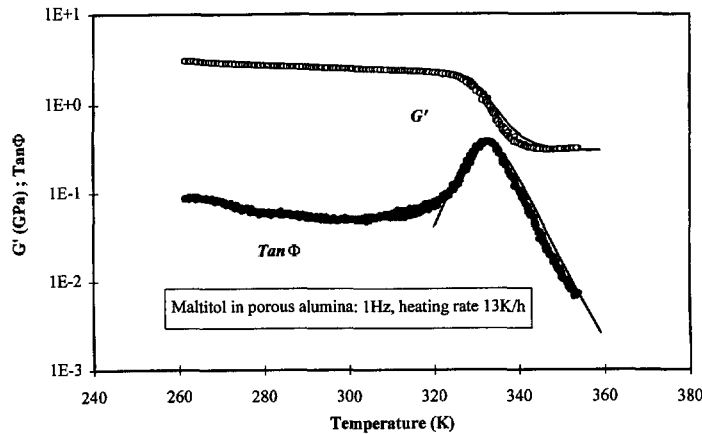


Fig. 6. — Mechanical loss tangent $\tan\phi$ and storage shear modulus G' of maltitol embedded in porous alumina measured as a function of temperature at 1 Hz. The full line corresponds to the modeling obtained by means of equations (3), (4) and (5), *via* procedure explained in Figure 8 and with parameters given in Table II.

of parameters given in the Table I. The effective time distribution g_i at 323 K is shown in the insert of Figure 4.

Lastly, from the relaxation map shown in Figure 5, it is worthwhile to determine the fragility parameter in the ergodic domain $m = \left. \frac{d \ln(\tau)}{dT_g/T} \right|_{T=T_g, T \geq T_g}$ as proposed by Angell [22]. m is close to 230 for maltitol. Consequently, this polyol can be considered as a fragile glass-forming system ($m = 46$ for SiO_2 and $m = 333$ for PMMA) [22]. It is important to note that the values quoted in this paper correspond to the fragility obtained for a time scale of 10^4 s as they are determined at $T_g(10^4 \text{ s})$. A way to relieve the fragility notion of the thermal activation contribution, is to consider the fragility parameter m' , defined as:

$$m' = \frac{E_{\text{app}}(T > T_g) - E_{\text{app}}(T < T_g)}{RT_g} \quad (6)$$

as previously proposed [23]. m' is only sensitive to the evolution of microstructure through the glass transition. One obtains $m' = 146$ for maltitol ($m' \approx 0$ for SiO_2 and $m' = 218$ for PMMA).

4. Viscoelastic Behavior of Maltitol Embedded Porous Alumina

The temperature dependence of G' and $\tan\phi$ of the composite sample is shown in Figure 6 and the master curves obtained through isothermal measurements are shown in Figures 7a and 7b. The following features are clearly observed in relation with the α -relaxation:

(i) the relaxed modulus G_r remains rather high (about 0.3 GPa). Actually it is an apparent modulus corresponding to the rigidity of porous alumina G_p containing maltitol in the supercooled liquid state;

(ii) as a consequence, $\tan\phi$ exhibits a peak instead of a monotonous increase;

(iii) the unrelaxed modulus G_u of the composite is lower than that of pure maltitol. This is unexpected since polycrystalline alumina has a much higher modulus than maltitol. This can be explained by the fact that some of the pores do not received maltitol. This is confirmed by density measurements which show that only a fraction of pores are filled with maltitol, *another*

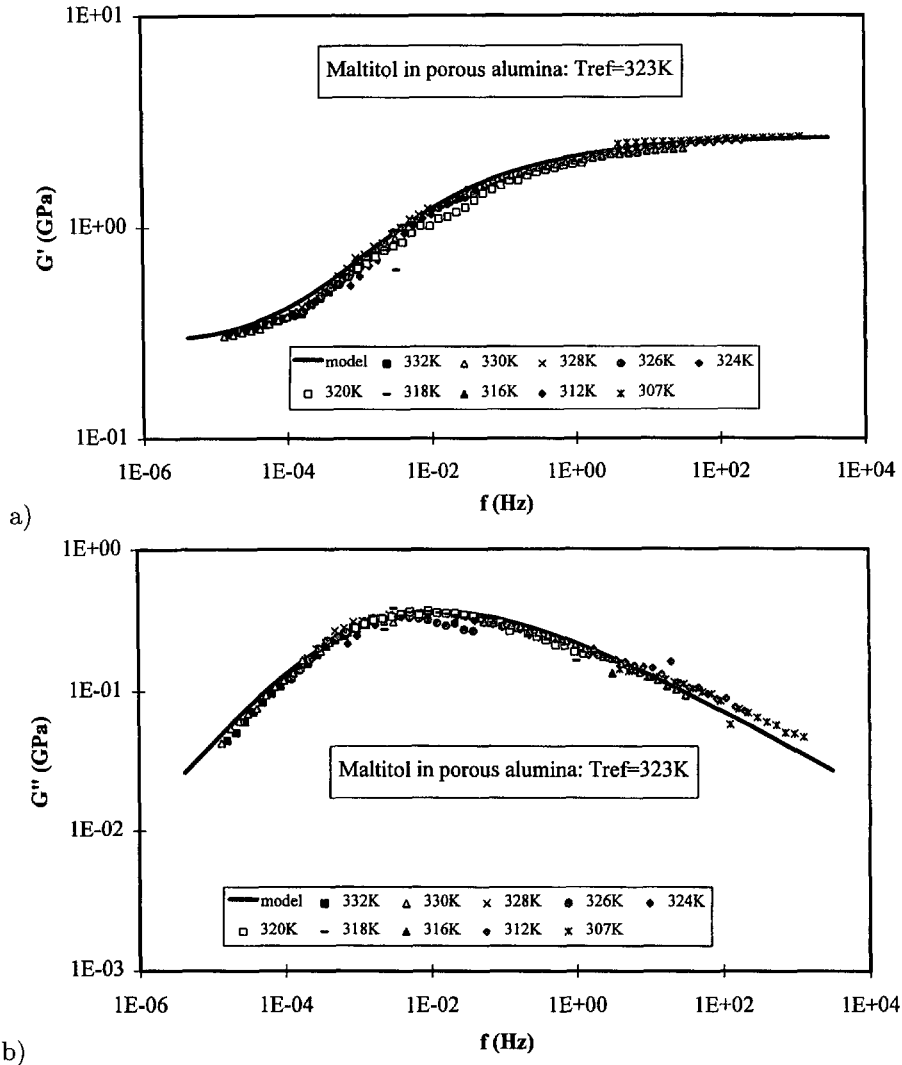


Fig. 7. — a) Master curve at 323 K built with data of G' measured at various temperatures for maltitol embedded in porous alumina. The full line corresponds to the modeling obtained with biparabolic expression *via* procedure explained in Figure 8. b) Master curve at 323K built with data of G'' measured at various temperature for maltitol embedded in porous alumina. The full lines correspond to the modeling obtained with biparabolic expression *via* procedure explained in Figure 8.

fraction f_{p0} remaining empty. This fact has to be taken into account in any mechanical model used to establish the relation between the measured dynamic modulus of composite sample and that of pure maltitol. We suggest a two-steps modeling for obtaining such a relation as shown in Figure 8.

First step:

The porous substrate is divided in two media, namely bulk alumina and air. Those media are considered to be mechanically coupled partly in series, partly in parallel [24]. Consequently, the two parameters λ_1 and ϕ_1 have to be introduced, and can be obtained from the following

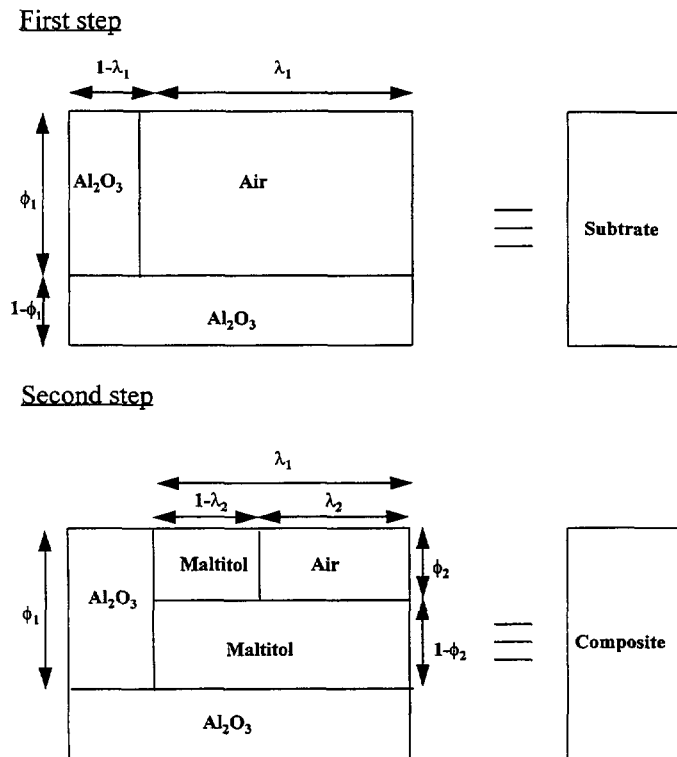


Fig. 8. — Modeling procedure for the composite sample. First step: series-parallel model for porous alumina. Second step: model for maltitol embedded in porous alumina.

relations:

$$\lambda_1 \phi_1 = f_p \tag{7a}$$

$$G_{Al_2O_3}(1 - \phi_1) = G_p \tag{7b}$$

f_p is the fraction of pores in the substrate ($f_p = 0.8$). $G_{Al_2O_3}$ which is close to 160 GPa and G_p close to 0.3 GPa are the modulus of polycrystalline alumina and porous alumina respectively.

Second step:

The part of the diagram corresponding to air (pores) is assumed to be partly filled with maltitol. Again, this is described by a parallel-series element with parameters λ_2 and ϕ_2 . These parameters account for the fraction of pores remaining empty after the introduction of maltitol in the substrate. They obey the following relations:

$$\lambda_2 \phi_2 = f_p f_{p0} \tag{7c}$$

$$G_{uc} = \frac{\phi_1}{\frac{1-\lambda_1}{G_{Al_2O_3}} + \frac{\lambda_1}{G_{eff}}} + (1 - \phi_1)G_{Al_2O_3} \tag{7d}$$

G_{uc} is the unrelaxed elastic modulus of the composite sample; G_{eff} is the effective unrelaxed modulus of maltitol occupying the fraction $1 - f_{p0}$ of the pores. G_{eff} is related to the unrelaxed modulus of maltitol, G_{um} , by:

$$G_{eff} = G_{um}(1 - \phi_2). \tag{7e}$$

Table II. — Values of the parameters involved in the modeling of the complex dynamic modulus of maltitol embedded in porous alumina, by means of biparabolic model and generalized Maxwell model (Appendix).

Composite: Maltitol in porous alumina	Generalized Maxwell Model	Biparabolic model
$G_{\text{Al}_2\text{O}_3}$ (GPa)	160	160
G_p (GPa)	0.3	0.3
G_{um} (GPa)	3×10^9	3×10^9
G_{uc} (GPa)	2.5×10^9	2.5×10^9
f_p	0.8	0.8
f_{p0}	0.3	0.3
χ	–	0.3
χ'	–	0.65
Q	–	0.3
$B_{\alpha\text{an}}$	0.42	–
$B_{\alpha\text{vp}}$	0.45	–

To sum up, after having measured G_{um} , G_{uc} , f_p , and f_{p0} , the relations (7a) to (7e) yield the parameters $\lambda_1 = 0.801$, $\phi_1 = 0.998$, $\lambda_2 = 0.246$, and $\phi_2 = 0.423$, which can be used to calculate the complex dynamic modulus $G^*(i\omega, T)$ for the composite medium as a function of the dynamic modulus $G_m^*(i\omega, T)$ of pure maltitol, through the relations:

$$G_c^*(i\omega, T) = \frac{\phi_1}{\frac{1-\lambda_1}{G_{\text{Al}_2\text{O}_3}} + \frac{\lambda_1}{G_{\text{eff}}^*(i\omega, T)}} + (1 + \phi_1)G_{\text{Al}_2\text{O}_3} \quad (8a)$$

and

$$G_{\text{eff}}^*(i\omega, T) = G_m^*(i\omega, T)(1 - \phi_2). \quad (8b)$$

Relations (8a) and (8b) correspond to equations (7d) and (7e), with $G_c^*(i\omega, T)$, $G_m^*(i\omega, T)$ and $G_{\text{eff}}^*(i\omega, T)$ instead of the unrelaxed elastic moduli. All the values of the used parameters are given in Table II.

Applying equations (8a) and (8b) with $G_m^*(i\omega, T)$ given by equation (3) as explained above, leads to the modeling of the Cole-Cole diagram of the composite sample shown in Figure 9. It appears that the calculated curve mostly differs from experimental data in the low frequency limit, as the calculated Cole-Cole plot exhibits a slope dG''/dG' which is higher than the experimental data. The maximum value of G'' is also overestimated. Nevertheless, a good agreement is obtained by decreasing the value of χ' , which is equal to 1 in the case of pure maltitol, down to 0.68 when maltitol is in porous alumina. The value χ is weakly affected (see Tab. I), and the corresponding slight variation can be attributed partly to the thermal history, which is not exactly the same for pure maltitol and the composite. It is worthwhile to note that the same conclusion can be reached, using the Maxwell model as explained in Appendix (see Tab. II). The change in the distribution of characteristic relaxation times is shown in the insert of Figure 9. It can be observed that this distribution is wider, and that the differences between the two distributions are essentially located in the long time range. However, the time position of the maxima of these distributions remain nearly the same.

Two reasons could explain the spreading of the distribution towards long times. It happens that the size of pores is distributed, from 10 μm down to less than 100 nm [12].

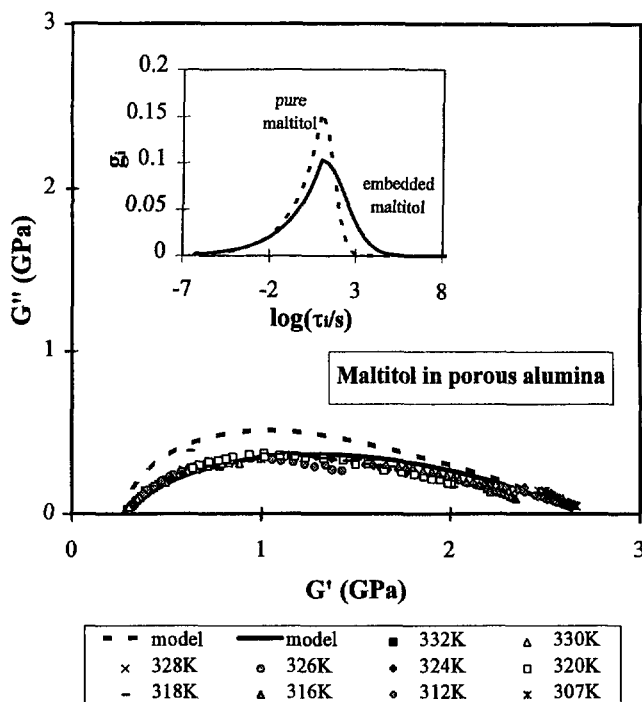


Fig. 9. — Cole-Cole representation of the isothermal data corresponding to maltitol embedded in porous alumina. The dotted line is the result bipolar model used *via* procedure explained in Figure 8 with parameters given in Table I. The full line corresponds to the same modeling with a new set of parameters given in Table II. *Insert*: distribution of the relaxation times τ_i obtained with equation (A.1) (Appendix) with the values of parameters given in Table I for dotted line and in Table II for the full line, respectively for bulk and embedded maltitol samples.

As a consequence:

(i) connection between pores are so narrow that some hydrodynamic effects could result in local flow becoming more difficult;

(ii) maltitol molecules could be likely to interact with the polar surface of pores and their mobility decreases. As the ratio surface/volume is high for small pores, such an effect concern a non-negligible number of molecules.

In both cases, a distribution of times wider in the long times side is to be expected, and self-consistent with the change displayed in the insert of Figure 9. The dynamics of molecular systems is known to be modified in confined geometry of small sizes (a few nanometers) [25,26]. For example, the dielectric relaxation shifts to lower temperatures or to higher frequencies, and confinement induces a broadening and a change in the shape of the relaxation spectrum [27]. In the case described here, the mean size of the pores is quite large, and the presence of the support only affects the long-time side of the distribution. As a consequence, the measured mean relaxation properties are relevant of the bulk product.

Lastly, the variation of τ_{mol} with temperature in the case of composite sample is also shown in Figure 5. It appears that the results can be hardly distinguished from those obtained with pure maltitol. This is understandable since the most probable value of the characteristic relaxation time is the same for bulk maltitol and composite sample distributions. Consequently, the time

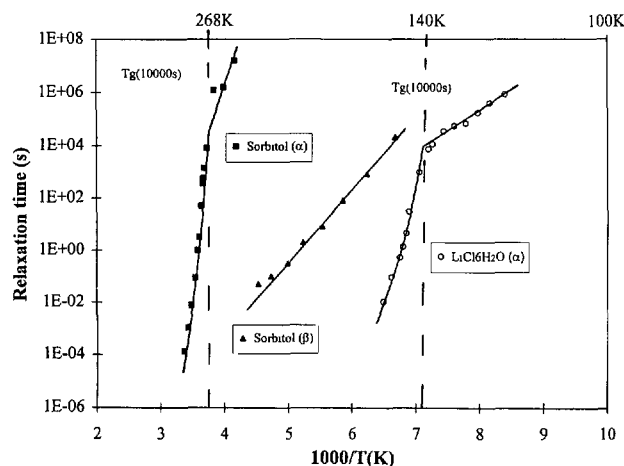


Fig. 10. — Relaxation map of sorbitol and LiCl. 6H₂O in the low frequency, and low temperature domains.

Table III. — Values of the apparent activation energies of the β -process and of the α -process in the isostructural state ($T < T_g$), and fragility parameters m and m' for maltitol, sorbitol and LiCl, 6H₂O.

	E_β (kJ/mol)	$E_{app}(T < T_g)$ (kJ/mol)	m (10 ⁴ s)	m' (10 ⁴ s)
Maltitol	62	200	230	146
Sorbitol	55	170	224	146
LiCl, 6H ₂ O	—	32	143	66

τ_{mol} characteristic of the molecular mobility of this molecular glass forming system can be determined from mechanical measurements performed on the so-called composite sample.

We have used the same porous substrate to determine the relaxation map of sorbitol and LiCl, 6H₂O. The calorimetric glass transition temperature of those systems are 270 K and 136 K [28] respectively, for a heating rate of 3×10^{-2} K/s, so that they are liquid at room temperature. The temperature variation of τ_{mol} obtained by means of mechanical measurement performed on sorbitol and LiCl, 6H₂O embedded in porous alumina is shown in Figure 10. This long times relaxation map reveals a fragile behavior for the α -relaxation in both systems. As for maltitol, an Arrhenius behavior is observed for temperatures below the glass transition $T_g(10^4$ s). Moreover, a sub- T_g Arrhenius β -relaxation process is observed for sorbitol, yielding to an activation energy analogous to that of maltitol. One can also determine the values of m and m' of these both systems. All values are present in Table III.

5. Conclusion

The dynamical mechanical behavior of a molecular glass forming system (maltitol) is described in this paper. Measurements were performed either on bulk samples and or on composite samples realized by injecting maltitol in a porous alumina substrate. A self-consistent description of all the experimental results was obtained by introducing parameters with physical meaning in phenomenological models. This yields a better understanding of the effects of the substrate on the dynamics of the embedded product. It appears that the long time exponent χ' of the

biparabolic expression is decreased, or equivalently that the distribution of the relaxation times spreads over the long time range, when maltitol is injected in porous alumina. Nevertheless, the most probable value of the relaxation time remains nearly the same.

On the basis of this study, an experimental procedure is established, allowing the determination of the low frequency dynamics, in the glassy state, as well as in the supercooled liquid, for systems with low glass transition temperatures. Comparison of the long time scale (10^{-1} s- 10^5 s) results obtained by means of this procedure with data issued from other spectroscopic techniques such as dielectric relaxation [29] enables the building of large relaxation maps [30], displaying the different relaxation processes of glass forming liquids on a wide temperature range below and above T_g . So far, the validity of the various models proposed in literature to describe the molecular mobility in the glass transition range can be reinvestigated on a wider time range. This will probably yield a better understanding of the nature of molecular motions in disordered systems.

Appendix

In order to bring a physical meaning to the phenomenological Maxwell description, it is possible to introduce τ_{mol} in equation (1). The problem is then to give an expression for g_i using parameters with physical meaning. Actually, if the values of the effective times τ_i are distributed around τ_{mol} , this can be accounted by considering a distribution of the parameter $1/\chi$ in equation (4a). This choice can be physically justified by the existence of long range spatial fluctuations of disorder, *i.e.* the defects concentration C_d , which should lead to variations in χ . If χ_m is defined as the most probable value of χ , the following distribution can be considered:

$$g_i^1 = \exp \left[-\frac{\left(\frac{1}{\chi_m} - \left(\frac{1}{\chi} \right)_i \right)}{B_{\alpha \text{ an}}} \right] \quad \text{for } 1 > \chi > \chi_m \quad (0 < i < n/2) \quad (\text{A.1a})$$

$$g_i^1 = \exp \left[-\frac{\left(\frac{1}{\chi_m} - \left(\frac{1}{\chi} \right)_i \right)^2}{B_{\alpha \text{ vp}}} \right] \quad \text{for } \chi < \chi_m \quad (n/2 < i < n) \quad (\text{A.1b})$$

with i : integer between $[0, n]$ and $\left(\frac{1}{\chi} \right)_i = 1 + \frac{1/\chi_m - 1}{n/2} i$.

The normalization condition leads to the value of g_i given by:

$$g_i = \frac{g_i^1}{\sum_{i=0}^n g_i^1} \quad (\text{A.1c})$$

The equation (A.1b) corresponds to a log-normal distribution of τ in the long time side, with a breadth parameter $B_{\alpha \text{vp}}$, while the equation (A.1a) gives a distribution of times decreasing with a long tail in the short time side. These expressions lead to a non-symmetric distribution function for the effective relaxation time, as it is generally recognized for α -relaxation.

Note added in the revised version: for sake of simplicity, a straight forward link is considered in the Appendix, between the well-known relation (1) and a distribution of relaxation times based on physical features. A more rigorous physical approach should have involved the analysis of the macroscopic mechanical response of the material to the applied stress, *i.e.*, the compliance

(or mechanical susceptibility $J^* = 1/G^*$), as a result of the sum of all microscopic responses. Two generalized Voigt models can be used for representing the non-elastic parts of this response, namely the anelastic and viscous components. The results are well-described using a Gumbel law [31] for the distribution of the anelastic retardation times and a Gaussian distribution for viscoplastic component, corresponding respectively to equations (A.1a and A.1b). Such an approach will be developed elsewhere. In any way, conclusions derived from the insert of Figure 9, remain the same.

References

- [1] McCrum N.G., Read B.E. and Williams G., Anelastic and dielectric effects in polymeric solids (J. Wiley & Sons Eds., 1967) 607p.
- [2] Etienne S. and Perez J., *Rev. Phys. Appl.* **14** (1979) 607.
- [3] Perez J., Duperray B. and Lefevre D., *J. Non-Cryst. Solids* **44** (1981) 113.
- [4] Lallemand J.P., Thesis, INSA-Lyon (1986) 196p.
- [5] Perez J., International Summer School on mechanical spectroscopy, Cracow Poland (Chapman Ed., 1991).
- [6] Ferry J.D., Viscoelastic properties of polymers (J. Wiley & Sons Eds., 1970) 2149p.
- [7] Cavaillé J.Y. and Perez J., *Phys. Rev. B* **39** (1989) 2411.
- [8] Cavaillé J.Y., Perez J. and Johari G.P., *J. Non-Cryst. Solids* **131-133** (1991) 935.
- [9] Maï C., Etienne S., Satha H. and Perez J., *Acta Metall. Mater.* **38** (1990) 337.
- [10] Vassoille R. and Perez J., *Ann. Phys. Fr.* **10** (1985) 307.
- [11] Etienne S., Cavaillé J.Y., Perez J., Point R., and Salvia M., *Rev. Sci. Instrum.* **53** (1982) 1231.
- [12] Massardier V., Thesis, INSA-Lyon (1994) 250p.
- [13] Havriliak S. and Negami S., *Polymer* **8** (1967) 161.
- [14] Cole K.S. and Cole R.H., *J. Chem. Phys.* **9** (1941) 341.
- [15] Fuoss R.M. and Kirkwood J.G., *J. Am. Chem. Soc.* **63** (1941) 385.
- [16] Davidson D.W. and Cole R.H., *J. Chem. Phys.* **18** (1950) 1417.
- [17] Alvarez F., Algeria A. and Colmenero J., *Phys. Rev. B* **47** (1993) 125.
- [18] Havriliak S. and Havriliak S.J., *J. Non-Cryst. Solids* **172-174** (1994) 297.
- [19] Decroix J.Y., Thesis, Université Claude Bernard, Lyon I (1974) 156p.
- [20] Diaz-Calleja R., Sanchis M.J. and Mostos J., *Polymer* **37** (1996) 4003.
- [21] Perez J., Physique et mécanique des polymères amorphes (Lavoisier, Paris, 1992) 374p.
- [22] Böhmer R., Ngai K.L., Angell C.A. and Plazek D.J., *J. Chem. Phys.* **99** (1993) 4201.
- [23] Perez J. and Cavaillé J.Y., *J. Non-Cryst. Solids* **172-174** (1994) 1028.
- [24] Takayanagi M., Harima H. and Iwata Y., *Mem. Fac. Eng. (Kyushu Univ.)* **23** (1963) 41.
- [25] Drake J.M. and Klafter J., *Phys. Today* **43** (1991) 46.
- [26] Jackson C.L. and McKenna G.B., *J. Non-Cryst. Solids* **131-133** (1991) 221.
- [27] Pissis P., Daoukaki-Diamanti D., Apekis L. and Christodoulides C., *J. Phys.: Condens. Matter* **6** (1994) L325.
- [28] Elarby A., Jal J.F., Chieux P., Letoffé J.M., Claudy P. and Dupuy-Philon J., *J. Non-Cryst. Solids* **104** (1988) 303.
- [29] Motosuke N. and Koji U., *J. Chem. Phys.* **99** (1993) 69.
- [30] Faivre A., David L., Vigier G., Niquet G., Maglione M., Maurin P.O., Jal J.F. and Dupuy-Philon J., *J. Chem. Phys.*, to be published.
- [31] Smith R.L., *Statistical Sci.* **4** (1989) 367.